Structural Engineering and Mechanics, Vol. 45, No. 1 (2013) 69 - 93
DOI: http://dx.doi.org/10.12989/sem.2013.45.1.069

On the dynamics of rotating, tapered, visco-elastic beams with a heavy tip mass

Serkan Zeren*[1] and Metin Gürgöze[2a]

[1]*Department of Mechanical Engineering, Yeditepe University, Istanbul, Turkey*
[2]*Faculty of Mechanical Engineering, Technical University of Istanbul, Istanbul, Turkey*

(Received January 12, 2012, Revised September 24, 2012, Accepted December 1, 2012)

Abstract. The present study deals with the dynamics of the flapwise (out-of-plane) vibrations of a rotating, internally damped (Kelvin-Voigt model) tapered Bernoulli-Euler beam carrying a heavy tip mass. The centroid of the tip mass is offset from the free end of the beam and is located along its extended axis. The equation of motion and the corresponding boundary conditions are derived via the Hamilton's Principle, leading to a differential eigenvalue problem. Afterwards, this eigenvalue problem is solved by using Frobenius Method of solution in power series. The resulting characteristic equation is then solved numerically. The numerical results are tabulated for a variety of nondimensional rotational speed, tip mass, tip mass offset, mass moment of inertia, internal damping parameter, hub radius and taper ratio. These are compared with the results of a conventional finite element modeling as well, and excellent agreement is obtained.

Keywords: rotating tapered beam; Bernoulli-Euler beam; Kelvin-Voigt material; heavy tip mass; offset

1. Introduction

Rotating cantilever beams with or without tip masses are found in several engineering applications. Dynamics of such beams have been studied by many researchers. Some of representative studies are given and outlined in the work of Gürgöze and Zeren (2009).

Further, Ozdemir Ozgumus and Kaya (2010) have investigated the flapwise vibrations of a tapered Timoshenko beam using differential transform method. Zhu (2011) has presented a modeling method of flapwise and chordwise vibrations analysis of rotating pre-twisted Timoshenko beams. In the work of Yan *et al*. (2011), an integral equation method was presented to analyze free vibrations of rotating nonuniform beams. Attarnejad and Shahba (2011a, b) have studied the free vibrations analysis of rotating tapered beams by introducing the concept of basic displacement functions in finite element method. Further, Zarrinzadeh *et al*. (2012) have improved the concept of basic displacement functions to the analysis of rotating beams made of axially functionally graded material. In the study of Shahba *et al*. (2011), a new beam element whose shape functions are expressed in basic displacement functions has been presented for free

∗Corresponding author, Graduate Research Assistant, E-mail: zerens@gmail.com
[a]Professor, E-mail: gurgozem@itu.edu.tr

vibrations analysis of rotating tapered functionally graded beams. Ganesh and Ganguli (2011) have developed new basis functions to solve the free vibrations problem for rotating beams by using finite element method. Gunda *et al*. (2007) have implemented a superelement based on a combination of polynomials and Fourier series to be used for vibration analysis of rotating structures. Banerjee *et al*. (2006) have investigated free vibrations of rotating tapered beams by using dynamic stiffness method. In Kumar and Ganguli (2011), the authors have studied rotating beams whose eigenpair (frequency and mode-shape) are same as that of uniform nonrotating beams for a particular mode with the aid of the flexural stiffness functions.

Generally speaking, most of these studies given above have focused mainly on the dynamics of rotating undamped beams without any tip mass. The publications (Abolghasemi and Jalali 2003, Younesian and Esmailzadeh 2010, Arvin and Bakhtiari-Nejad 2011) are considered also with rotating beams in which nonlinear oscillations are investigated.

Unlike the articles above, the beam considered in the work of Gürgöze and Zeren (2011) has a tip mass and more importantly, the interest there lies in establishing the "exact" characteristic Eq. of a rotating visco-elastic beam (Kelvin-Voigt model) such that its eigenvalues can be obtained.

Table 1 The effect of the nondimesional rotational speed $\overline{\Omega}$ on the nondimensional fundamental eigenvalues $\overline{\lambda}_{1,2}$ of a rotating tapered beam sytem shown in Fig. 1 for the values of the nondimensional parameters $\alpha_M = \overline{d} = \overline{R} = \overline{c} = \overline{J}_s = 0$, $\eta = 0.95$ and $\mu = 0.8$

$\overline{\Omega}$	$\overline{\lambda}_{1,2}$	ω_1
0	±5.2738i **±5.2738i**	5.2738
1	±5.3904i **±5.3904i**	5.3903
2	±5.7249i **±5.7249i**	5.7249
3	±6.2403i **±6.2403i**	6.2402
4	±6.8929i **±6.8929i**	6.8928
5	±7.6444i **±7.6444i**	7.6443
6	±8.4653i **±8.4654i**	8.4653
7	±9.3347i **±9.3348i**	9.3347
8	±10.2380i **±10.2380i**	10.2379
9	±11.1651i **±11.1652i**	11.1650
10	±12.1092i **±12.1093i**	12.1092
11	±13.0657i **±13.0658i**	13.0657
12	±14.0313i **±14.0314i**	14.0313

Table 2 The nondimensional eigenvalue pairs $\overline{\lambda}_{1,2}$ of the rotating uniform beam system shown in Fig. 1 for various values of the nondimensional rotational speed, tip mass and hub parameter $\overline{\Omega}$, α_M, $\overline{R}$, with $\bar{c} = 0.01$, $\bar{J}_s = 0.01$, $\bar{d} = 0.1$, $\eta = 0$, and $\mu = 0$

$\overline{R}$	$\overline{\Omega}$	$\alpha_M = 0.1$	$\alpha_M = 1$	$\alpha_M = 2$	$\alpha_M = 5$
0	0	-0.412355 ± 2.842019i **-0.412418 ± 2.842230i**	-0.116375 ± 1.521167i **-0.116394 ± 1.521300i**	-0.064686 ± 1.135578i **-0.064697 ± 1.135680i**	-0.027729 ± 0744182i **-0.027734 ± 0.744237i**
	1	-0.412413 ± 3.034221i **-0.412475 ± 3.034420i**	-0.116646 ± 1.867320i **-0.116666 ± 1.867420i**	-0.065176 ± 1.570604i **-0.065187 ± 1.570670i**	-0.028699 ± 1.313332i **-0.0287043 ± 1.31337i**
	2	-0.413195 ± 3.547170i **-0.413257 ± 3.547310i**	-0.119638 ± 2.636432i **-0.119658 ± 2.636500i**	-0.069626 ± 2.430450i **-0.069637 ± 2.430490i**	-0.034546 ± 2.255252i **-0.034551 ± 2.25527i**
	3	-0.416066 ± 4.263066i **-0.416128 ± 4.263180i**	-0.127709 ± 3.549652i **-0.127729 ± 3.549700i**	-0.079169 ± 3.387034i **-0.079181 ± 3.387060i**	-0.043352 ± 3.239944i **-0.0433567 ± 3.23996i**
	4	-0.422278 ± 5.093395i **-0.422340 ± 5.093460i**	-0.140305 ± 4.511377i **-0.140325 ± 4.511410i**	-0.091605 ± 4.369141i **-0.091617 ± 4.369160i**	-0.052923 ± 4.2338031i **-0.0529281 ± 4.23381i**
	5	-0.432483 ± 5.987762i **-0.432544 ± 5.987790i**	-0.155712 ± 5.492063i **-0.155732 ± 5.492080i**	-0.105183 ± 5.360395i **-0.105194 ± 5.360400i**	-0.062582 ± 5.231095i **-0.0625869 ± 5.2311i**
	10	-0.535049 ± 10.799539i **-0.535104 ± 10.799500i**	-0.241539 ± 10.470287i **-0.241558 ± 10.470300i**	-0.172434 ± 10.354736i **-0.172444 ± 10.354700i**	-0.108151 ± 10.234035i **-0.107662 ± 10.23400i**
0.01	0	-0.412356 ± 2.842019i **-0.412418 ± 2.842230i**	-0.116375 ± 1.521167i **-0.116394 ± 1.521300i**	-0.064686 ± 1.135578i **-0.0646974 ± 1.135680i**	-0.027728 ± 0.744182i **-0.0277337 ± 0.744237i**
	1	-0.412414 ± 3.036479i **-0.412476 ± 3.03666i**	-0.116650 ± 1.870602i **-0.116670 ± 1.870720i**	-0.065184 ± 1.574407i **-0.0651951 ± 1.574480i**	-0.028714 ± 1.317734i **-0.0287194 ± 1.31777i**
	2	-0.413206 ± 3.554866i **-0.413269 ± 3.55501i**	-0.119683 ± 2.645569i **-0.119703 ± 2.645630i**	-0.069689 ± 2.439996i **-0.0697011 ± 2.440040i**	-0.034619 ± 2.25064i **-0.0346241 ± 2.26509i**
	3	-0.416111 ± 4.277408i **-0.416173 ± 4.27752i**	-0.127834 ± 3.564662i **-0.127854 ± 3.56471i**	-0.079313 ± 3.402094i **-0.0793246 ± 3.40212i**	-0.043478 ± 3.254943i **-0.0434835 ± 3.25495i**
	4	-0.422387 ± 5.114635i **-0.422448 ± 5.114690i**	-0.140517 ± 4.532096i **-0.140537 ± 4.532120i**	-0.091819 ± 4.389584i **-0.091831 ± 4.389600i**	-0.053094 ± 4.253937i **-0.0530994 ± 4.25394i**
	5	-0.432678 ± 6.015875i **-0.43274 ± 6.0159100i**	-0.155996 ± 5.518402i **-0.156017 ± 5.518410i**	-0.105452 ± 5.386174i **-0.105464 ± 5.38618i**	-0.062792 ± 5.256351i **-0.0627967 ± 5.25635i**
	10	-0.535747 ± 10.861033i **-0.535802 ± 10.860900i**	-0.241992 ± 10.524437i **-0.242011 ± 10.524400i**	-0.172867 ± 10.407082i **-0.172878 ± 10.407100i**	-0.075274 ± 10.200542i **-0.108010 ± 10.284800i**
0.05	0	-0.412355 ± 2.842019i **-0.412418 ± 2.842230i**	-0.116375 ± 1.521167i **-0.116394 ± 1.52130i**	-0.064686 ± 1.135578i **-0.0646974 ± 1.13568i**	-0.027728 ± 0.744182i **-0.027733 ± 0.744237i**
	1	-0.412417 ± 3.045494i **-0.412479 ± 3.045700i**	-0.116668 ± 1.883671i **-0.116688 ± 1.883790i**	-0.065217 ± 1.589521i **-0.065228 ± 1.589590i**	-0.028775 ± 1.335186i **-0.028780 ± 1.335220i**
	2	-0.413253 ± 3.585482i **-0.413315 ± 3.585680i**	-0.119862 ± 2.681791i **-0.119882 ± 2.681870i**	-0.069946 ± 2.477791i **-0.069957 ± 2.477840i**	-0.034909 ± 2.303867i **-0.034914 ± 2.303890i**
	3	-0.416297 ± 4.334289i **-0.416359 ± 4.334460i**	-0.128333 ± 3.624054i **-0.128354 ± 3.624120i**	-0.079885 ± 3.46146i **-0.079897 ± 3.461690i**	-0.043980 ± 3.314224i **-0.043985 ± 3.314240i**
	4	-0.422829 ± 5.198708i **-0.422892 ± 5.198890i**	-0.141359 ± 4.614004i **-0.141380 ± 4.614070i**	-0.092667 ± 4.470381i **-0.092679 ± 4.470420i**	-0.053771 ± 4.333503i **-0.053777 ± 4.333520i**
	5	-0.433473±6.126999i **-0.433536±6.127190i**	-0.157128±5.622483i **-0.157149±5.622540i**	-0.106519±5.488042i **-0.106531±5.488080i**	-0.063621 ± 5.356150i **-0.063626 ± 5.356170i**
	10	-0.538628 ± 11.103470i **-0.538690 ± 11.103700i**	-0.243796 ± 10.738248i **-0.243817 ± 10.738300i**	-0.174582 ± 10.613837i **-0.174593 ± 10.613900i**	-0.188134 ± 10.098788i **-0.109380 ± 10.485600i**

Table 2 Continued

0.1	0	-0.412355 ± 2.842019i **-0.412418 ± 2.842230i**	-0.116375 ± 1.521167i **-0.116394 ± 1.521300i**	-0.064686 ± 1.135578i **-0.064697 ± 1.135680i**	-0.027728 ± 0.744182i **-0.027734 ± 0.744237i**
	1	-0.412422 ± 3.056724i **-0.412484 ± 3.056930i**	-0.116691 ± 1.899878i **-0.116711 ± 1.899990i**	-0.65259 ± 1.608205i **-0.065270 ± 1.608270i**	-0.028853 ± 1.356662i **-0.028858 ± 1.356700i**
	2	-0.413313 ± 3.623382i **-0.413375 ± 3.623540i**	-0.120091 ± 2.726364i **-0.120110 ± 2.726440i**	-0.070269 ± 2.524192i **-0.070280 ± 2.524230i**	-0.035269 ± 2.351408i **-0.035274 ± 2.351430i**
	3	-0.416537 ± 4.404334i **-0.416599 ± 4.404430i**	-0.128958 ± 3.696894i **-0.128978 ± 3.696940i**	-0.080595 ± 3.534602i **-0.080607 ± 3.534630i**	-0.044597 ± 3.386795i **-0.044602 ± 3.386810i**
	4	-0.423398 ± 5.301880i **-0.42346 ± 5.301950i**	-0.142403 ± 4.714313i **-0.142423 ± 4.714340i**	-0.093709 ± 4.569285i **-0.093721 ± 4.569300i**	-0.054600 ± 4.430879i **-0.054606 ± 4.430880i**
	5	-0.434495 ± 6.263059i **-0.434556 ± 6.263080i**	-0.158522 ± 5.749850i **-0.158542 ± 5.749860i**	-0.107828 ± 5.612691i **-0.107840 ± 5.612700i**	-0.064635 ± 5.478269i **-0.064640 ± 5.478270i**
	10	-0.542415 ± 11.398987i **-0.54247 ± 11.398900i**	-0.246029 ± 10.999546i **-0.246049 ± 10.999500i**	-0.176683 ± 10.866651i **-0.176693 ± 10.866600i**	-0.134548 ± 10.744433i **-0.111049 ± 10.731300i**

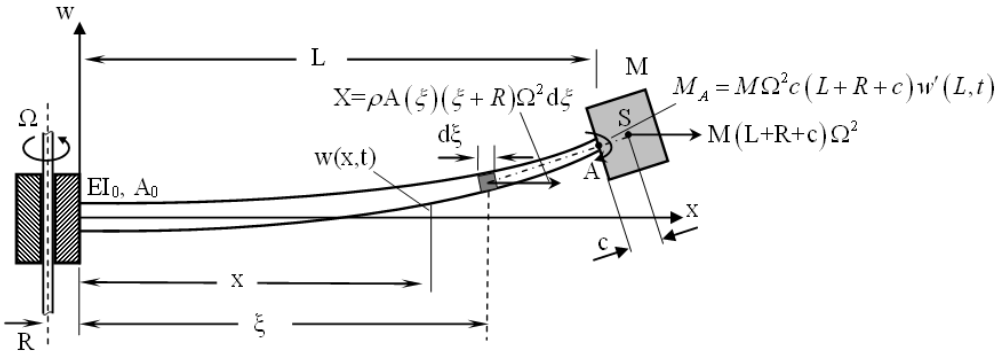

Fig. 1 Rotating tapered visco-elastic Bernoulli-Euler beam carrying a heavy tip mass

The study of Gürgöze and Zeren (2011) represents to some extent a more general form of Gürgöze and Zeren (2009) in that in the latter study, mass of moment of inertia and offset of the tip mass are taken into consideration, as well.

The present study is an extension of the above study in that the beam here is assumed to be tapered and is attached to a hub, through which a more realistic model is supplied for many practical applications, even though in a very simplified form. To the best knowledge of the present authors, the characteristic equation derived here and the numerical results obtained from it, have not previously been given in the technical literature. Therefore, Table 1 and Table 2 contain ample numerical results which provide researchers with the opportunity to compare their work on the dynamics of rotating beams. Apart from Table 1 and Table 2 serving as reference material, some of the numerical results are given in the form of graphs, as well.

2. Theory

The system examined, shown schematically in Fig. 1 is a beam of variable cross section, carrying a so called heavy tip mass *M.* Its mass moment of inertia with respect to the perpendicular

axis at the centroid S is denoted by J_S. The centroid S of the tip mass is offset by c from the free end of the beam and is located along its extended axis. The beam attached to a hub with radius R is rotating around the vertical axis with constant angular velocity $\overline{\Omega}$. The beam is made of a visco-elastic material (Kelvin-Voigt model).

It is assumed that the effects of shear deformations and rotary inertia are neglected, in other words, Euler-Bernoulli Beam is considered. Further, it is assumed that the cross section of the rotating beam is doubly symmetric and consequently, the shear center and geometric centers are coincident. As is known, this leads to the simplification that the displacements along y and z axes, i.e., in-plane and out-of-plane bending displacements and the twist angle are uncoupled. Additionally, it is also assumed that the breadth/thickness ratio is high, such that the more dominant out-of-plane vibrations of the rotating beam need to be investigated only. Differently from the work of Gürgöze and Zeren (2011), it is assumed here that the beam has a variable cross section along its length in the form of a taper, and furthermore, it is attached to a hub of radius R.

2.1 Derivation of the Eq. of motion and the boundary conditions

Gürgöze and Zeren (2011) have derived the Eq. of motion by using the classical method, i.e., via the formulation of the bending moment at a cross section of the beam and then taking the appropriate partial derivatives. In the present study, however, the Hamilton's Principle is employed for the derivation of the equation of motion and the corresponding boundary conditions, as it enables one to obtain the equation of motion and the corresponding boundary conditions in a very systematic manner. Additionally, it is more suitable for further generalizations of the present mechanical system which the authors plan to do.

One can write the extended form of the Hamilton's Principle with the notations used in the present study as

$$\int_{t_0}^{t_1}\left[\delta\left(T-U\right)+\delta W+\delta' A\right]\mathrm{d}t=0 \tag{1}$$

In the above expression, T denotes the total kinetic energy of the system and the term U contains both potential energy and work of centrifugal forces along the x axis. The term δW represents the virtual work done by the moment of the inertial forces of the tip mass M. Finally, $\delta' A$ indicates the virtual work of the non-conservative forces.

Total kinetic energy T

$$T=T_1+T_2 \tag{2}$$

consists of the following parts

$$\begin{aligned} T_1&=\int_0^L\frac{1}{2}\rho A\left(x\right)\dot{w}^2\left(x,t\right)\mathrm{d}x,\\ T_2&=\frac{1}{2}Mv_S^2+\frac{1}{2}J_S\dot{w}'^2\left(L,t\right). \end{aligned} \tag{3}$$

T_1 and T_2 denote here the kinetic energies of the beam and of the tip mass M, respectively. In the above expressions, J_S indicates mass moment of inertia of the tip mass with respect to the

perpendicular axis at the centroid *S*. The out-of-plane bending displacements are denoted by the function $w(x,t)$ where *x* and *t* denote location of the beam element and time, respectively. ρ and $A(x)$ represent mass density and variable cross section of the beam respectively. The over dot and prime denote respectively partial differentiation with respect to time *t* and longitudinal coordinate *x*.

Velocity of the centroid of the tip mass v_S in z-direction is written as follows

$$v_S = \dot{w}(L,t) + c\dot{w}'(L,t) \tag{4}$$

Potential energy of the system includes two parts, one for bending and the other due to the work of centrifugal forces along the *x* axis

$$U = U_1 + U_2 \tag{5}$$

The term U_1 can be written as

$$U_1 = \int_0^L \frac{1}{2} EI(x) w''^2(x,t)\,\mathrm{d}x \tag{6}$$

The work done by the centrifugal forces along the x axis is

$$U_2 = \int_0^L \frac{w'^2(x,t)}{2} X^*(x,t)\,\mathrm{d}x \tag{7}$$

In the last expression, X^* represents the resultant of the axial inertial forces acting at the right of the differential element along the *x* axis due to rotating. Axial displacements due to bending (the so called, foreshortening) can be shown to be $w'^2(x,t)/2$ (Meirovitch 1967). The force X^* consists of the sum of two axial force components as shown in Fig. 1: Namely, the sum of the axial inertial forces acting on the differential element $d\xi$ indicated by *X* and inertial forces of the tip mass

$$X^*(x,t) = \int_x^L \rho A(\xi)(\xi + R)\Omega^2 \mathrm{d}\xi + M\Omega^2(L + R + c) \tag{8}$$

The term δW can be expressed as

$$\delta W = M_A \delta w'(L,t) \tag{9}$$

where M_A indicates the moment of the axial inertial forces of the tip mass with respect to point *A*, as shown in Fig. 1.

The term M_A can be written as

$$M_A = M\Omega^2 c(L + R + c) w'(L,t) \tag{10}$$

Finally, the work done by the non-conservative forces, i.e., damping forces, can be expressed as follows

$$\delta' A = -\int_V \sigma_{damp} \delta\varepsilon \mathrm{d}V \tag{11}$$

In the present study, the damping stresses obey Kelvin-Voigt model as stated previously

$$\sigma_{damp} = \alpha\dot{\varepsilon} \tag{12}$$

where α represents the visco-elastic constant of the beam material (Banks and Inman 1991). Here, the dot above the term indicates the derivative with respect to time *t*. According to Bernoulli-Euler beam theory, strain of a fiber of the beam can be expressed as

$$\varepsilon = z\kappa + \varepsilon_0 \tag{13}$$

where $\kappa \approx \partial^2 w(x,t)/\partial x^2$, ε_0 and z indicate the curvature of the beam, strain at the centerline and the distance from the centerline to the fiber in the curvature plane respectively (Stevens 1966). The expression (11) can be written with the help of the expressions of (12) and (13) as

$$\delta' A = -\int_0^L \alpha I(x)\dot{w}''(x,t)\delta w''(x,t)\,\mathrm{d}x \tag{14}$$

Substituting expressions (2), (5), (9), and (14) into (1), carrying out the necessary variations, and after lengthy operations, the following partial differential Eq. of fifth order with variable coefficients is obtained as the Eq. of motion of the beam

$$\begin{aligned}&\left[EI(x)w''(x,t)+\alpha I(x)\dot{w}''(x,t)\right]'' - \left[\int_x^L (R+\xi)\rho A(\xi)\Omega^2 w'(x,t)\,d\xi\right]' \\ &-M(L+R+c)\Omega^2 w''(x,t)+\rho A(x)\ddot{w}(x,t)=0.\end{aligned} \tag{15}$$

The corresponding boundary conditions are as follows

$$w(0,t)=0 \tag{16}$$

$$w'(0,t)=0 \tag{17}$$

$$EI(L)w''(L,t)+\alpha I(L)\dot{w}''(L,t)+M\Omega^2(L+R+c)cw'(L,t)+\left(J_S+Mc^2\right)\dot{w}'(L,t)+Mc\ddot{w}(L,t)=0 \tag{18}$$

$$\left[EI(x)w''(x,t)+\alpha I(x)\dot{w}''(x,t)\right]'_{x=L} - M\ddot{w}(L,t)-Mc\ddot{w}'(L,t)-M(L+R+c)\Omega^2 w'(L,t)=0 \tag{19}$$

The boundary conditions (16) and (17) represent deflection and rotation at $x=0$ while the Eqs. (18) and (19) are balance-expressions between the bending moment and rotation of the inertia element and shear force with inertia force.

2.2 Derivation of the eigenvalue problem

Differential Eq. (15) and the boundary conditions (16)-(19) set up a boundary value problem (Meirovitch 1967). Assume a solution of this problem in the following form

$$w(x,t)=W(x)e^{\lambda t} \tag{20}$$

In the above expression, $W(x)$ and λ are the amplitude function and the corresponding eigenvalue, respectively. They are both complex in general. Substituting (20) into the partial differential Eq. (15) and the boundary conditions (16)-(19), yields

$$\left[EI(x)W''(x)+\alpha I\left(x\right)\lambda W''(x)\right]''-\Omega^2\left[W'(x)\int_x^L\left(R+\xi\right)\rho A\left(\xi\right)d\xi\right]' \\ -\left(L+R+c\right)M\Omega^2W''\left(x\right)+\rho A\left(x\right)\lambda^2W(x)=0, \tag{21}$$

$$W(0)=0 \tag{22}$$

$$W'(0)=0 \tag{23}$$

$$\left(EI(L)+\alpha I(L)\lambda\right)W''(L)+M\Omega^2\left(L+R+c\right)cW'(L)+\left(J_S+Mc^2\right)\lambda^2W'(L)+Mc\lambda^2W(L)=0 \tag{24}$$

$$\left[\left(EI(x)+\alpha I(x)\lambda\right)W''\left(x\right)\right]'_{x=L}-M\Omega^2\left(L+R+c\right)W'(L)-M\lambda^2W(L)=0 \tag{25}$$

Ordinary differential Eq. (21) and the boundary conditions (22)-(25) establish a differential eigenvalue problem for the continuous system shown in Fig. 1. It is reasonable to write down the above differential equation and the boundary conditions in a non-dimensional form. After lengthy algebraic manipulations, the above differential eigenvalue problem can be expressed as

$$\left[f(\bar{x})\bar{W}''(\bar{x})\right]''-a\left[\bar{W}''(\bar{x})\int_{\bar{x}}^1\left(\bar{R}+\bar{\xi}\right)g\left(\bar{\xi}\right)d\bar{\xi}-\left(\bar{R}+\bar{x}\right)g\left(\bar{x}\right)\bar{W}'\left(\bar{x}\right)\right] \\ -\left(1+\bar{R}+\bar{c}\right)\alpha_M a\bar{W}''(\bar{x})+bg\left(\bar{x}\right)\bar{W}(\bar{x})=0 \tag{26}$$

$$\bar{W}(0)=0 \tag{27}$$

$$\bar{W}'(0)=0 \tag{28}$$

$$f(1)\bar{W}''(1)+2\alpha_M a\left(1+\bar{R}+\bar{c}\right)\bar{c}\bar{W}'(1)+b\left(\bar{J}_s+\alpha_M\bar{c}^2\right)\bar{W}'(1)+b\alpha_M\bar{c}\bar{W}(1)=0 \tag{29}$$

$$\left[f(\bar{x})\bar{W}''(\bar{x})\right]'\Big|_{\bar{x}=1}-\alpha_M\left[b\bar{c}+2a\left(1+\bar{R}+\bar{c}\right)\right]\bar{W}'(1)-\alpha_M b\bar{W}(1)=0 \tag{30}$$

where the following non-dimensional quantities are introduced

$$\bar{x}=x/L,\quad \bar{\xi}=\xi/L,\quad \bar{W}=W/L,\quad \bar{c}=c/L,\quad \bar{R}=R/L \\ {\omega_0}^2=EI_0/\rho A_0L^4,\quad \bar{\Omega}=\Omega/\omega_0,\quad \bar{\lambda}=\lambda/\omega_0 \\ d=\alpha I_0/L^3,\quad \bar{d}=d/\rho A_0L\omega_0 \\ \alpha_M=M/\rho A_0L,\quad \bar{J}_s=J_s/\rho A_0L^3 \\ a=\bar{\Omega}^2/2(1+\bar{d}\bar{\lambda}),\quad b=\bar{\lambda}^2/(1+\bar{d}\bar{\lambda}) \tag{31}$$

In addition, the new functions $f(x)$ and $g(x)$ indicate the changes of the second moment of cross sectional area $I(x)$ and area of the cross section $A(x)$ along x axis, respectively

$$I(x)=I_0f(x),\quad A(x)=A_0g(x) \tag{32}$$

2.3 Series solution of the eigenvalue problem

In this section, we seek the solution to the differential eigenvalue problem introduced above. The solution procedure aims to find values of the parameter $\overline{\lambda}$ for which there are nonvanishing amplitude functions $\overline{W}(\overline{x})$ satisfying the differential Eq. (26) and the corresponding boundary conditions (27)-(30). Frobenius method of solution in power series is a suitable method, as the differential Eq. (26) has variable coefficients. For a linearly tapered beam, the functions $f(x)$ and $g(x)$ can be represented as

$$\begin{aligned} f(\overline{x}) &= 1-\eta\overline{x} \\ g(\overline{x}) &= 1-\mu\overline{x} \end{aligned} \tag{33}$$

Now, the solution in power series can be expressed as

$$\overline{W}(\overline{x}) = \sum_{n=0}^{\infty} C_n \overline{x}^{n+r} \tag{34}$$

where C_n represent unknown coefficients which are interrelated via recurrence relationships. To obtain these recurrence relationships, one can substitute the solution (34) into the differential Eq. (26) and then, the following expression can be obtained, after lengthy operations

$$C_0(r-3)(r-2)(r-1)r = 0 \tag{35}$$

Some details of the derivation are given in an Appendix. In the above equation, *r* can take values 0, 1, 2, and 3. Consequently, the solution can be expressed in the form of four linearly independent functions

$$u_r(\overline{x}) = \sum_{n=0}^{\infty} C_n{}^r \overline{x}^{n+r} \quad \text{(r = 0, 1, 2, 3).} \tag{36}$$

For unknown coefficients $C_n{}^r$, the following recurrence relationships depending on *r*, can be obtained

$$C_1{}^r = \frac{\eta C_0{}^r (r-1)}{(r+1)} \tag{37}$$

$$C_2{}^r = \frac{\eta C_1{}^r (r+1)(r) + C_0{}^r a\left[\gamma + \alpha_M (1+\overline{R}+\overline{c})\right]}{(r+2)(r+1)} \tag{38}$$

$$C_3{}^r = \frac{\eta C_2{}^r (r+1)^2 + C_1{}^r a\left[\gamma + \alpha_M (1+\overline{R}+\overline{c})\right](r+1) - C_0{}^r a\overline{R} r}{(r+3)(r+2)(r+1)} \tag{39}$$

$$C_4^r = \frac{\eta C_3 (r+2)^2 (r+3) + C_2 a\left[\gamma + \alpha_M (1+\overline{R}+\overline{c})\right](r+2) - C_1 a\overline{R}(r+1) - 1/2\, C_0 a(1-\mu\overline{R})r - bC_0}{(r+4)(r+3)(r+2)(r+1)} \tag{40}$$

$$C_n{}^r = \frac{\eta(n+r+2)}{n+r} C_{n-1}{}^r + \frac{a\left[\gamma + \alpha_M(1+R+\bar{c})\right]}{(n+r-1)(n+r)} C_{n-2}{}^r - \frac{a\bar{R}(n+r-3)}{(n+r-2)(n+r-1)(n+r)} C_{n-3}{}^r$$
$$- \frac{1/2\, a(1-\mu\bar{R})(n+r-4)(n+r-3)+b}{(n+r-3)(n+r-2)(n+r-1)(n+r)} C_{n-4}{}^r + \frac{1/3\, a\mu(n+r-5)(n+r-3)+b}{(n+r-3)(n+r-2)(n+r-1)(k+r)} C_{n-5}{}^r \quad (41)$$
(n=5, 6,…)

It is seen from (37) to (41) that all unknown $C_n{}^r$ coefficients can be written in terms of $C_0{}^r$. However, the coefficients $C_0{}^r$ are arbitrary, so they can be chosen as "one".

Via the recurrence relationships (37)-(41), the solution (34) in power series can be rearranged as

$$\bar{W}(\bar{x}) = \sum_{r=0}^{3} A_r u_r(\bar{x}) = A_0 u_0(\bar{x}) + A_1 u_1(\bar{x}) + A_2 u_2(\bar{x}) + A_3 u_3(\bar{x}) \quad (42)$$

The four linearly independent functions $u_0(\bar{x})$ to $u_3(\bar{x})$ in the above expression, can be written as

$$u_0(\bar{x}) = 1 - \eta\bar{x} + \frac{a\left[\gamma + \alpha_M(1+\bar{R}+\bar{c})\right]}{2}\bar{x}^2 \ldots\ldots \quad (43)$$

$$u_1(\bar{x}) = \bar{x} + \frac{a\left[\gamma + \alpha_M(1+\bar{R}+\bar{c})\right]}{2}\bar{x}^3 \ldots \quad (44)$$

$$u_2(\bar{x}) = \bar{x}^2 + \frac{\eta}{3}\bar{x}^3 + \frac{2\eta^2 + a\left[\gamma + \alpha_M(1+\bar{R}+\bar{c})\right]}{12}\bar{x}^4 \ldots \quad (45)$$

$$u_3(\bar{x}) = \bar{x}^3 + \frac{\eta}{2}\bar{x}^4 + \frac{6\eta^2 + a\left[\gamma + \alpha_M(1+\bar{R}+\bar{c})\right]}{20}\bar{x}^5 \ldots \quad (46)$$

where the new abbreviation

$$\gamma = \frac{1}{2} + \bar{R} - \mu\left(\frac{1}{3} + \frac{\bar{R}}{2}\right) \quad (47)$$

is introduced.

Use of the boundary conditions (27) and (28) and the formulas (43)-(47) in (42) leads to

$$\bar{W}(0) = A_0 = 0 \quad (48)$$

$$\bar{W}'(0) = A_1 = 0 \quad (49)$$

So, the general solution (42) reduces to

$$\bar{W}(\bar{x}) = A_2 u_2(\bar{x}) + A_3 u_3(\bar{x}) \quad (50)$$

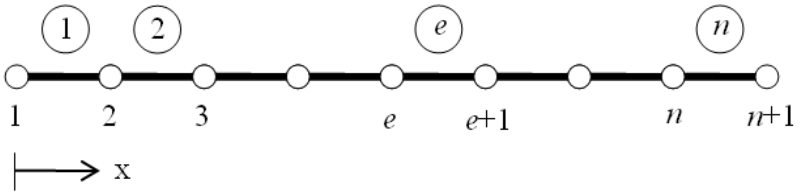

Fig. 2 Numbering the elements and nodes of the finite element model

The boundary conditions (29) and (30) can be expressed in matrix notation as

$$\begin{bmatrix} p_{22} & p_{23} \\ p_{32} & p_{33} \end{bmatrix} \begin{bmatrix} A_2 \\ A_3 \end{bmatrix} = \begin{bmatrix} 0 \\ 0 \end{bmatrix} \tag{51}$$

where the element functions are given as

$$p_{2k}\left(\bar{\lambda}\right) = f(1)u_k''(1) + 2\alpha_M a\left(1+\bar{R}+\bar{c}\right)\bar{c}u_k''(1) + b\left(\bar{J}_s + \alpha_M \bar{c}^2\right)u_k'(1) + b\alpha_M \bar{c}u_k(1) = 0 \tag{52}$$

$$p_{3k}\left(\bar{\lambda}\right) = \left[f(\bar{x})u_k''(\bar{x})\right]'\Big|_{\bar{x}=1} - \alpha_M\left[b\bar{c} + 2a\left(1+\bar{R}+\bar{c}\right)\right]u_k'(1) - \alpha_M b u_k(1) = 0 \tag{53}$$

with $k = 2, 3$ and the prime denotes derivatives with respect to $\bar{x}$. For a non-trivial solution pair of A_2 and A_3, the determinant of the square matrix in (51) must be equal to zero

$$p_{22}p_{33} - p_{23}p_{32} = 0 \tag{54}$$

The values of the parameter $\bar{\lambda}$ which satisfy this characteristic equation, give the nondimensional eigenvalues of the rotating, tapered visco-elastic beam with a tip mass having an offset as shown in Fig. 1. To determine these values, the elements $p_{2k}(\bar{\lambda})$ and $p_{3k}(\bar{\lambda})$ with $k = 2, 3$ are computed according to the expressions given in (52) and (53), using a sufficient number of terms in the series (34), employing MATLAB's "fsolve" function.

In order to be able to validate the numerical results that will be obtained from the procedure above, a finite element model of the system will be established in the following section.

2.4 Finite element modeling

For finite element analysis, the rotating beam is discretized into n elements with two-nodes shown in Fig. 2 where the numbers above and below the beam represent the corresponding element and node numbers, respectively. The transverse displacements of an element can be approximated by a cubic polynomial with four constants

$$w(x) = a_1 + a_2 x + a_3 x^2 + a_4 x^3 = \begin{bmatrix} 1 & x & x^2 & x^3 \end{bmatrix} \begin{bmatrix} \alpha_1 \\ \alpha_2 \\ \alpha_3 \\ \alpha_4 \end{bmatrix} \tag{55}$$

In the above expressions, x and α_i indicate the spatial coordinate and unknown constants, respectively. An element has two nodes and a node has two degrees of freedom: transverse displacement and slope

$$w(x_e) = w_e, \quad \left.\frac{\partial w}{\partial x}\right|_{x=x_e} = \theta_e \tag{56}$$

Displacements of the element e can be written in vector form as

$$\mathbf{d_e} = \left[w_e, \theta_e, w_{e+1}, \theta_{e+1}\right]^{\mathbf{T}} \tag{57}$$

In the above expression, x_e and x_{e+1} denote the spatial coordinates of the node at the left end and right end, respectively.

The transverse displacements of the eth element can be expressed as

$$w(x) = \mathbf{N}\mathbf{d}_e \tag{58}$$

where **N** is the vector whose elements are the well known cubic Hermite shape functions

$$\begin{aligned}
N_1(x) &= (x - x_{e+1})^2 (2x - 3x_e + x_{e+1}) / h_e^3, \\
N_2(x) &= (x - x_e)(x - x_{e+1})^2 / h_e^2, \\
N_3(x) &= -(x - x_e)^2 (2x + x_e - 3x_{e+1}) / h_e^3, \\
N_4(x) &= (x - x_e)^2 (x - x_{e+1}) / h_e^2.
\end{aligned} \tag{59}$$

In the above expressions, h_e indicates the length of the eth element. Substituting the expression (58) into (3) leads to the kinetic energy of eth element

$$T_e = \frac{1}{2}\dot{\mathbf{d}}_e^T \left(\int_{x_e}^{x_{e+1}} \rho A(x) \mathbf{N}^T \mathbf{N} \mathrm{d}x \right) \dot{\mathbf{d}}_e \tag{60}$$

From the above expression, the element mass matrix can be obtained as

$$\mathbf{m}_e = \int_{x_e}^{x_{e+1}} \rho A(x) \mathbf{N}^T \mathbf{N} \mathrm{d}x \tag{61}$$

The element potential energy can be written with the help of the expressions (6) and (58) as

$$U_{1_e} = \frac{1}{2}\mathbf{d}_e^T \left(\int_{x_e}^{x_{e+1}} EI(x) \mathbf{N}''^T \mathbf{N}'' \mathrm{d}x \right) \mathbf{d}_e \tag{62}$$

The element stiffness matrix is introduced as

$$\mathbf{k}_e = \int_{x_e}^{x_{e+1}} EI(x) \mathbf{N}''^T \mathbf{N}'' \mathrm{d}x \tag{63}$$

Other element matrices are given below

$$\mathbf{c}_e = \int_{x_e}^{x_{e+1}} \alpha I(x)\mathbf{N}''^T\mathbf{N}''\mathrm{d}x, \quad \mathbf{s}_e = \int_{x_e}^{x_{e+1}} H(x)\mathbf{N}'^T\mathbf{N}'\mathrm{d}x, \quad \bar{\mathbf{m}}_e = \int_{x_e}^{x_{e+1}} M\left(L+R+c\right)\mathbf{N}'^T\mathbf{N}'\mathrm{d}x. \quad (64)$$

In the above expression, the function $H\left(x\right)$ is defined as

$$H(x) = \int_{x}^{L} \rho A\left(\xi\right)\left(\xi + R\right)\mathrm{d}\xi \quad (65)$$

The above element matrices are assembled in the conventional way to form the global matrices

$$\mathbf{M} = \overset{n}{\underset{e=1}{A}}\mathbf{m}_\mathbf{e}, \quad \mathbf{K} = \overset{n}{\underset{e=1}{A}}\mathbf{k}_\mathbf{e}, \quad \mathbf{C} = \overset{n}{\underset{e=1}{A}}\mathbf{c}_\mathbf{e}, \quad \mathbf{S} = \overset{n}{\underset{e=1}{A}}\mathbf{s}_\mathbf{e}, \quad \mathbf{M}_\mathbf{L} = \overset{n}{\underset{e=1}{A}}\bar{\mathbf{m}}_\mathbf{e} \quad (66)$$

Implementation of the boundary conditions at the right end of the beam introduces some additional terms to the indicated elements of the global matrices **M** and **K**

$$\begin{aligned} M(2n+1,2n+1) &\triangleq +M \\ M(2n+1,2n+2) &\triangleq +Mc \\ M(2n+2,2n+1) &\triangleq +Mc \\ M(2n+2,2n+2) &\triangleq J_S + Mc^2 \\ K(2n+2,2n+2) &\triangleq +M\Omega^2 c(R+L+c) \end{aligned} \quad (67)$$

Finally, the quadratic eigenvalue problem can be formulated in terms of the above global matrices

$$\left\{\lambda^2\mathbf{M} + \lambda\mathbf{C} + \left[\mathbf{K} + \Omega^2\left(\mathbf{S} + \mathbf{M}_\mathbf{L}\right)\right]\right\}\mathbf{d} = \mathbf{0}, \quad (68)$$

where λ and Ω denote eigenvalues and rotational speed of the beam, respectively. The eigenvalue problem is numerically solved using the well known software MATHEMATICA.

3. Numerical evaluations

This section is devoted to the discussion of the numerical solution of the characteristic Eq. obtained in the previous section. Fig. 3 represents the convergence features of the nondimensional eigenvalue of the rotating beam for a set of nondimensional parameters shown in the figure. The solid line in the figure indicates the exact value of the nondimensional eigenvalue (Wright et al. 1982). It is seen from the figure that the use of 200 terms in the series solution of the characteristic Eq. (54) is sufficient to obtain converged numerical results. So all numerical calculations based on the series solution (34) are conducted by using 200 terms.

The nondimensional "first" eigenvalues, or more properly the pair of eigenvalues, of the mechanical system in Fig. 1 are given in Table 1 and 2 for various nondimensional system parameters: $\overline{\Omega}$, α_M, $\overline{d}$, $\overline{R}$, $\overline{c}$, $\overline{J}_S$, η, μ. In Table 1, the effect of the rotational speed on the non-

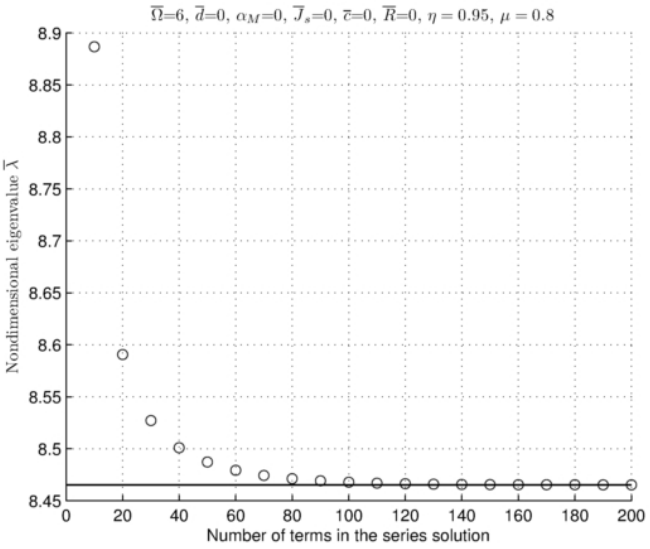

Fig. 3 The convergence test

dimensional eigenvalues of a rotating tapered beam is investigated. In the second column, the values of the pair of eigenvalues $\overline{\lambda}_{1,2}$ in the first row of each cell are the results based on the series solution of the characteristic Eq. (54). The bold values in the second row of each cell in the second column are the simulation results obtained by the conventional finite element method. The number of the terms used in the series solution (34) is 200, whereas 50 elements were used during the finite element calculations.

Eigenvalues have only imaginary parts due to the absence of the internal damping. (i.e., $\overline{d} = 0$). The comparison of both complex numbers in each cell of the second column shows that the agreement of solutions from series solution and finite element method is very good. The values ω_1 in the third column are taken from Table 5 of the study of Wright *et al*. (1982) which is probably one of the most cited works in the field of rotating beams. Excellent agreement of the values in the second and third column verifies the formulas established in this study. Table 1 reveals the fact that magnitudes of the imaginary parts of the nondimensional eigenvalues increase for increasing values of the rotational speed.

Another numerical application is to investigate the effect of the nondimensional hub radius $\overline{R}$ on the eigenvalues $\overline{\lambda}_{1,2}$ of a rotating uniform beam. The eigenvalues corresponding to various values of the parameter $\overline{R}$ are given in Table 2 for certain ranges of nondimensional angular velocity $\overline{\Omega}$ and tip mass parameter α_M. Remaining nondimensional parameters are selected as: $\overline{d} = 0.1$ and $\overline{c} = \overline{J}_S = 0.01$. Table 2 shows that for other parameter ranges chosen, the system is "oscillatory damped" as the first pairs of eigenvalues corresponding to this region are fully complex numbers. Table 2 reveals that the real parts of the nondimensional eigenvalues increase for increasing values of the nondimensional hub parameter when the angular velocity and mass of the tip mass are kept constant. The real parts of the eigenvalues are related to internal damping of the system, so increase of the hub radius strengthens the damping effect. Additionally, increase of the hub radius results in an increase in the absolute values of the imaginary parts of the

eigenvalues of the system, as expected.

Some numerical results based on the series solution of the characteristic Eq. (54) are given in Figs. 4-7. In Fig. 4, various values of the cross section parameters η and μ, tip mass parameter α_M and corresponding eigenvalues of the system are illustrated for a range of nondimensional rotating velocity $\overline{\Omega}$. For the smallest value of the tip mass parameter α_M (Fig. 4(a_1)), absolute values of the real parts of the eigenvalues increase as the cross section parameters η and μ increase. The taper ratio strongly affects the stiffness of the beam. As expected, the stiffness of the beam decreases as the taper ratio increases. This results in increasing the damping effect. This trend is more evident at higher rotation velocities and for the highest taper ratio ($\eta = 0.95$, $\mu = 0.80$). On the contrary, when the nondimensional tip mass parameter gets larger, increase of the cross section parameters η and μ weakens the damping effect. (Figs. 4(b_1), 4(c_1) and 4(d_1)). The weakening of the damping effect is more evident at low rotational speeds. Higher rotational speeds counteract this effect.

From Figs. 4(a_2) to 4(d_2), it is seen that increasing mass of the tip mass leads to a moderate decrease of the absolute value of the imaginary parts of the eigenvalues, i.e., the increase of the mass of the system leads the complex eigenfrequencies decrease. The change of the taper ratio has very little effect on the complex eigenfrequencies of the system. For the configuration in which the tip mass parameter is selected as 0.1 in Fig. 4(a_2), as the taper ratio gets larger, the complex frequencies of the system increases in the range of $\overline{\Omega}$ values up to 4. In contrast, the complex frequencies get smaller as the cross section parameters get larger at rotational speeds higher than 4.

Fig. 5 represents the effect of the damping parameter, i.e., visco-elastic constant and the cross section parameters on the eigenvalues. In this figure, offset parameter $\overline{c}$, the tip mass moment inertia parameter $\overline{J}_S$, and hub parameter $\overline{R}$ are taken as 0.01, whereas the tip mass parameter α_M is chosen as 0.1. Damping parameter $\overline{d}$ takes the values 0, 0.01, 0.1 and 0.5, respectively in Figs. 5(a)-5(d_1), and 5(d_2). The following can be observed from these figures: The complex eigenfrequencies increase slightly as the taper ratio increases in the range of the rotational speed $\overline{\Omega}$ up to 4. There is a node at $\overline{\Omega} \approx 4$ where all cross section parameters yield the same value for the eigenvalues. Behind this point, the increment of the rotational speed leads to smaller complex eigenfrequencies, as the taper ratio gets larger. The maximal decrement arises at the configuration in which the taper ratio has its greatest value as represented by the bold solid curves in Figs. 5(a)-5(c_2). When the damping ratio attains its largest value 0.5 as in Fig. 5(d_2), cross section parameters have no further influence on the values of the imaginary parts of the eigenvalues: The complex eigenfrequencies increase as the rotational speed increases, as the system becomes stiffer.

The increase of the damping parameter $\overline{d}$ leads to an increase of the internal damping of the system as expected. (Figs. 5(b_1)-5(d_1)). It is also seen from these figures that generally, higher taper ratios strengthen damping effect in the mechanical system shown in Fig. 1.

It is seen from Figs. 5(b_1) and 5(c_1), that the vertical distance between each $\left|\text{Real}\left(\overline{\lambda}_{1,2}\right)\right|$ curve is nearly constant in the region of the rotational speed $\overline{\Omega}$ up to 4. For larger rotational speeds, the highest taper ratio ($\eta = 0.90$, $\mu = 0.80$) leads to the maximal increment of the internal damping of the system. To sum up, it can be stated that higher taper ratios strengthen damping effect of the viscoelatic beam especially at higher rotational speeds.

The fact obviously seen from Figs. 5(b_2)-5(d_2) is that the increase of the taper ratio slightly increase the complex eigenfrequencies up to some rotational speed ($\overline{\Omega} \approx 4$).This issue could be explained by considering that herewith both of stiffness and mass parameters decrease. In contrast,

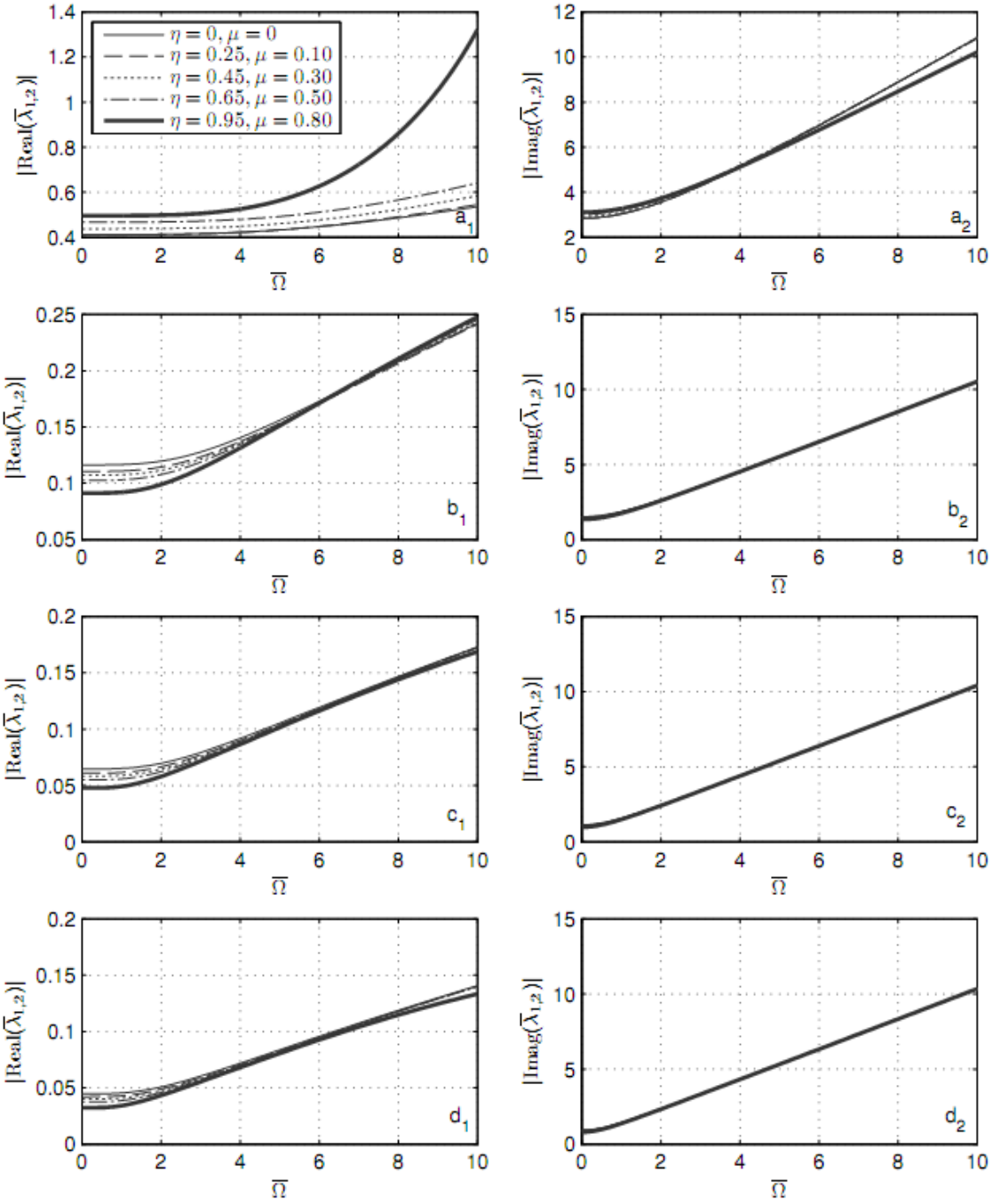

Fig. 4 Influence of the beam cross section parameters η, μ and the tip mass parameter α_M on the nondimensional eigenvalues $\bar{\lambda}_{1,2}$ depending upon the nondimensional rotational speed $\bar{\Omega}$, where: offset parameter $\bar{c} = 0.01$, mass moment of inertia of the tip mass parameter $\bar{J}_S = 0.01$, hub parameter $\bar{R} = 0.01$, and damping parameter $\bar{d} = 0.1$. (a_1), (a_2): tip mass parameter $\alpha_M = 0.1$; (b_1), (b_2): $\alpha_M = 1$; (c_1), (c_2): $\alpha_M = 2$; (d_1), (d_2): $\alpha_M = 3$

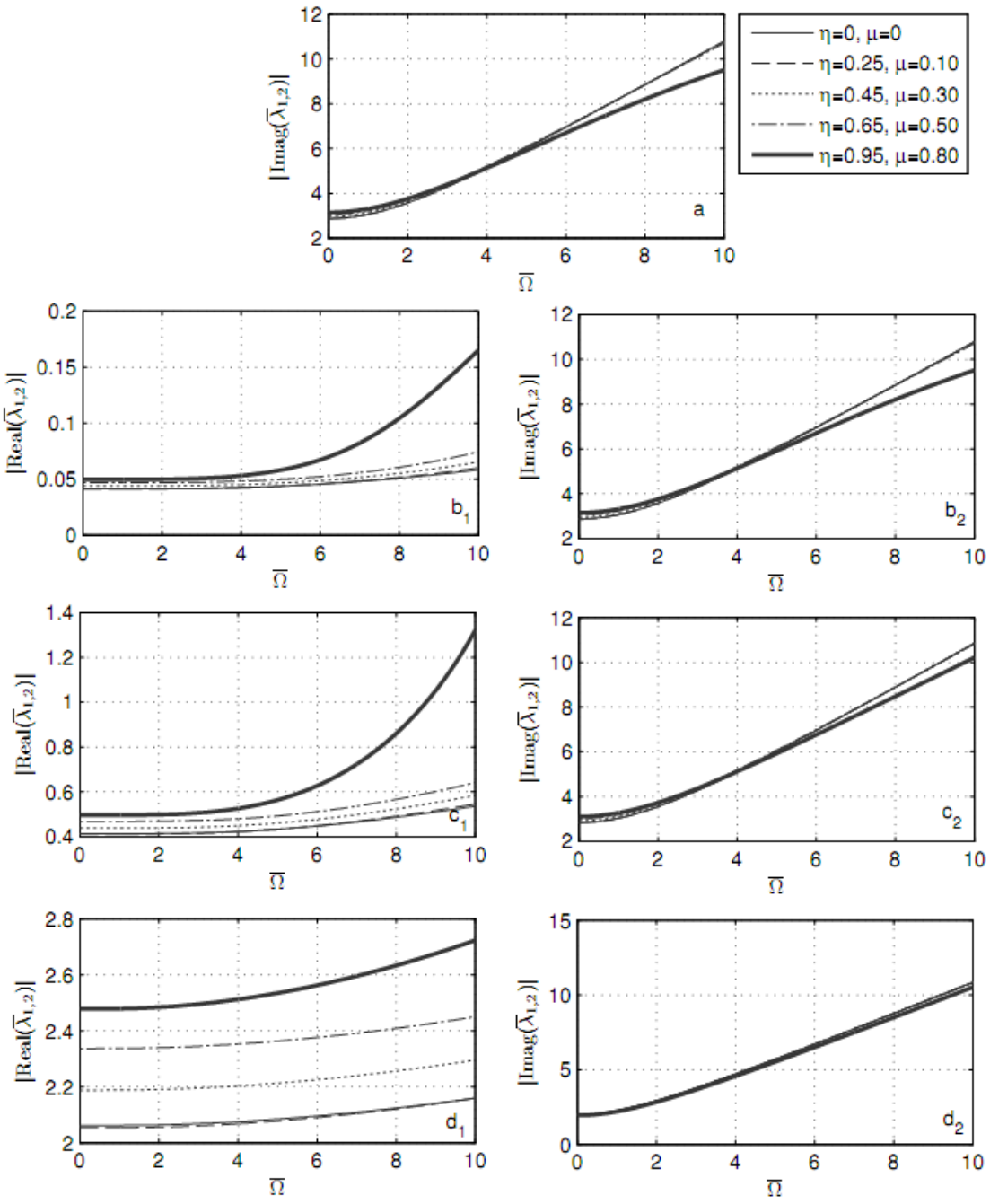

Fig. 5 Influence of the beam cross section parameters η, μ and the nondimensional damping parameter $\bar{d}$ on the nondimensional eigenvalues $\bar{\lambda}_{1,2}$ depending upon the nondimensional rotational speed $\bar{\Omega}$, where: offset parameter $\bar{c} = 0.01$, mass moment of inertia of the tip mass parameter $\bar{J}_S = 0.01$, hub parameter $\bar{R} = 0.01$ and tip mass parameter $\alpha_M = 0.1$. (a): $\bar{d} = 0$; (b_1), (b_2): $\bar{d} = 0.01$; (c_1), (c_2): $\bar{d} = 0.1$; (d_1), (d_2); $\bar{d} = 0.5$

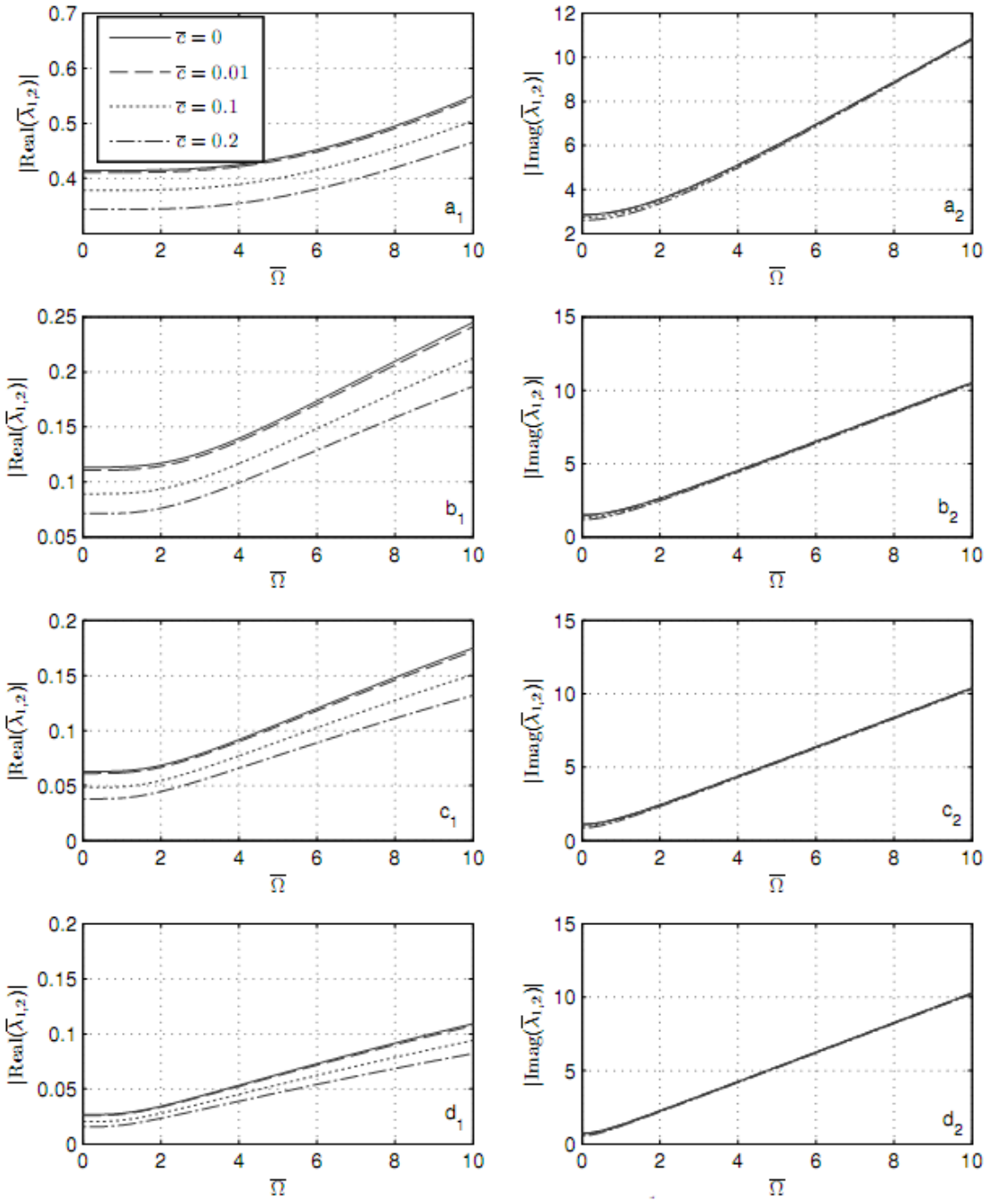

Fig. 6 Influence of the offset parameter $\bar{c}$ on the nondimensional eigenvalues $\bar{\lambda}_{1,2}$ depending upon the nondimensional rotational speed $\bar{\Omega}$, where: mass moment of inertia of the tip mass parameter $\bar{J}_S = 0.01$, hub parameter $\bar{R} = 0.01$, damping parameter $\bar{d} = 0.1$, and cross section parameters $\eta = 0.25$, $\mu = 0.1$; (a_1), (a_2): tip mass parameter $\alpha_M = 0.1$; (b_1), (b_2): $\alpha_M = 1$; (c_1), (c_2): $\alpha_M = 2$; (d_1), (d_2): $\alpha_M = 5$

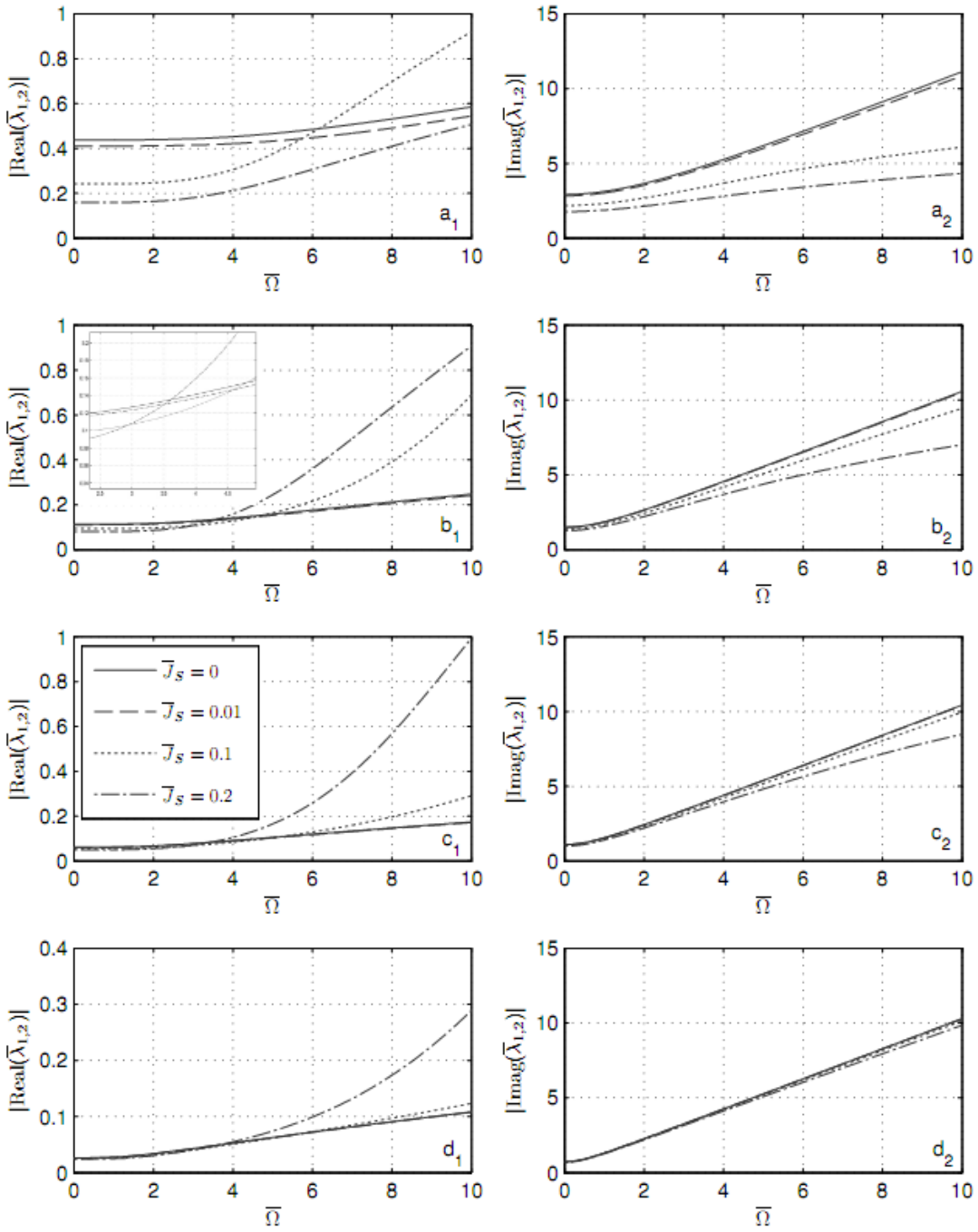

Fig. 7 Influence of the mass moment of inertia of the tip mass parameter $\bar{J}_S$ on the nondimensional eigenvalues $\bar{\lambda}_{1,2}$ depending upon the nondimensional rotational speed $\bar{\Omega}$, where: offset parameter $\bar{c} = 0.01$, hub parameter $\bar{R} = 0.01$, damping parameter $\bar{d} = 0.1$, and the cross section parameters $\eta = 0.25$, $\mu = 0.1$.(a_1), (a_2): tip mass parameter $\alpha_M = 0.1$; (b_1), (b_2): $\alpha_M = 1$; (c_1), (c_2): $\alpha_M = 2$; (d_1), (d_2): $\alpha_M = 5$

for higher rotational speeds, higher taper ratios cause a decrease in the complex eigenfrequencies as the system becomes less stiff. This effect is more evident when damping parameter $\bar{d}$ is taken as 0.01 and 0.1 as shown in Figs. 5(b_2) and 5(c_2). It is seen that for the largest damping parameter, cross section parameters have no considerable influence on the complex eigenfrequencies at small rotational speeds up to 6. As the rotational speed increases, the increase of the taper ratio causes the complex eigenfrequencies to decrease slightly.

In order to visually emphasize the influences of the offset parameter $\bar{c}$ and mass moment of inertia $\bar{J}_S$ of the tip mass on the eigenvalues $\bar{\lambda}_{1,2}$, the absolute values of the real and imaginary parts of $\bar{\lambda}_{1,2}$ are depicted in Figs. 6 and 7 as functions of the rotational speed $\bar{\Omega}$, for some selected values of the remaining physical parameters. In Fig. 6, the mass moment of inertia of the tip mass parameter $\bar{J}_S$ and the hub radius parameter $\bar{R}$ are taken as 0.01. Damping parameter $\bar{d}$ is 0.1 and cross section parameters η and μ are selected as 0.25 and 0.1, respectively. The tip mass parameter α_M takes the values 0.1, 1, 2 and 5 in Figs. 6(a_1), 6(a_2) to 6(d_1), and 6(d_2), respectively. The increase of the offset parameter $\bar{c}$ weakens the damping effect, as the effective mass increases when the offset is increased. The offset parameter $\bar{c}$ has very little influence on the imaginary parts of the eigenvalues. The effective mass increases as the offset is increased. It is seen from Figs. 6(a_1)-6(d_1) that as the tip mass parameter α_M gets larger, the damping effect diminishes.

In Fig. 7, the mass moment of inertia of the tip mass parameter $\bar{J}_S$ takes the values 0, 0.01, 0.1 and 0.2. The tip mass parameter α_M is selected as 0.1, 1, 2 and 5 in Figs. 7(a_1), 7(a_2) to 7(d_1), 7(d_2). In Fig. 7(a_1), at low rotational speeds, increase of the mass moment of inertia of the tip mass parameter $\bar{J}_S$ weakens the damping effect to a large extent. Generally, the $\left|\text{Real}\left(\bar{\lambda}_{1,2}\right)\right|$-curves rise and get closer as the rotational speed gets larger. There is one exception, however: For $\bar{J}_S = 0.1$, the absolute values of the real parts of the eigenvalues increase much more as the rotational speed parameter $\bar{\Omega}$ increases, and takes the maximum value at the largest rotational speed. As the tip mass parameter α_M gets larger (Figs. 7(b_1)-7(d_1)), the damping effect weakens. This point is in agreement with the findings of Gürgöze *et al*. (2007) where a non-rotating cantilevered visco-elastic beam carrying a tip mass was represented by a spring-damper-mass, i.e., a one-degree-of-freedom system. For small values of the mass moment of inertia of the tip mass parameter $\bar{J}_S$, the $\left|\text{Real}\left(\bar{\lambda}_{1,2}\right)\right|$-curves rise slightly as the rotational speed increases. On the contrary, larger values of $\bar{J}_S$ like 0.1, and 0.2 lead to the strengthening of the damping effect much more at high rotational speeds. But this effect is suppressed as the tip mass parameter α_M gets larger, as it is seen from Fig. 7(d_1).

Finally, from Figs. 7(a_2)-7(d_2) it is seen that the complex eigenfrequencies increase as the rotational speed increases. Inspection of Figs. 7(a_2)-7(d_2) reveals that the increase of the values of $\bar{J}_S$ leads to a decrease in the complex frequencies. This effect is more dominant for small values of the tip mass parameter α_M (Figs. 7(a_2) and 7(b_2)). As the parameter α_M gets larger, the effect of the parameter $\bar{J}_S$ on the eigenfrequencies weakens. For the largest value of the parameter α_M, $\left|\text{Imag}\left(\bar{\lambda}_{1,2}\right)\right|$-curves are almost identical.

4. Conclusions

This study investigated the out-of-plane (flapwise) vibrations of a rotating visco-elastic non-

uniform beam carrying a heavy tip mass. The heavy tip mass possesses a mass moment of inertia and its centroid is offset from the free end of the beam. The cross section of the beam is doubly symmetric and hence, in-plane and out-of plane displacements and twist angle can be assumed to be uncoupled. Additionally, it is assumed that the out-of-plane displacements are dominant for a slender beam like the one investigated in this study. The significant contribution of this study is to obtain the exact characteristic Eq. of the mechanical system that is made of a centrifugally stiffened, visco-elastic non-uniform (tapered) Bernoulli-Euler beam with a heavy tip mass. To the best knowledge of the authors, characteristic equation of this system has not been given previously in the technical literature.

The "fundamental" eigenvalue pairs obtained from the characteristic Eq. above and finite element model are tabulated for various physical system parameters. Some numerical results are also given in graphical form in order to better put forward visually the influences of taper ratio of cross section of the beam, damping parameter and tip mass parameter on the eigenvalues. Inspection of the numerical results shows clearly that the offset and the mass moment of inertia of the tip mass, taper ratio of the beam and hub radius may affect considerably the eigencharacteristics of rotating beams carrying a heavy tip mass. Hence, these parameters must be seriously considered in modeling of the rotating beam systems.

Some of the findings of this study regarding the influence of various physical parameters on the eigencharacteristics of a rotating beam can be summarized as follows:

- The increase of the rotational speed of the beam causes the complex eigenfrequencies to increase, as herewith the beam will be stiffer through the increasing centrifugal forces.
- When the tip mass increases, the complex eigenfrequencies gets smaller, as expected.
- At higher rotational speeds, the increase of the mass moment of inertia causes the complex eigenfrequencies to decrease, as herewith the effective mass increases.
- The increase of the taper ratio strengthens the damping effect, as the taper ratio strongly effects the stiffness of the beam.
- The increase of the tip mass and offset parameters weakens the damping effect. The effect of increasing of the offset parameter is the same as increasing tip mass.
- At lower rotational speeds, increase of the mass moment of inertia of the tip mass and the increase of the taper ratio for larger tip mass values, weaken the damping effect.

References

Abolghasemi, M. and Jalali, M.A. (2003)**,** "Attractors of a Rotating Viscoelastic Beam", *International Journal of Non-Linear Mechanics*, **38**, 739-751.

Arvin, H. and Bakhtiari-Nejad, F. (2011), "Non-linear modal analysis of a rotating beam", *International Journal of Non-Linear Mechanics*, **46**, 877-897.

Attarnejad, R. and Shahba, A. (2011a), "Dynamic basic displacement functions in free vibration analysis of centrifugally stiffened tapered beams; a mechanical solution" *Meccanica*, **46,** 1267-1281.

Attarnejad, R. and Shahba, A. (2011b), "Basic displacement functions for centrifugally stiffened tapered beam", *International Journal of Numerical Methods in Biomedical Engineering,* **27**, 1385-1397.

Banerjee, J.R., Su, H. and Jackson, D.R. (2006), "Free vibration of a rotating tapered beams using the dynamic stiffness method", *Journal of Sound and Vibration*, **298**, 1034-1054.

Banks, H.T. and Inman, D.J. (1991), "On Damping Mechanisms in Beams", *Journal of Applied Mechanics*,

58, 716-723.
Ganesh, R. and Ganguli, R. (2011), "Physics based basis function for vibration analysis of high speed rotating beams". *Structural Engineering and Mechanics*, **39**, 21-46.
Gunda, J.B., Singh, A.P., Chhabra, P.S. and Ganguli, R. (2007), "Free vibration analysis of rotating tapered blades using Fourier-p superelement", *Structural Engineering and Mechanics*, **27**, 243-257.
Gürgöze, M., Dogruoglu, A.N. and Zeren, S. (2007), "On the eigencharacteristics of a cantilevered visco-elastic beam carrying a tip mass and its representation by a spring-damper-mass system", *Journal of Sound and Vibration*, **301**, 420-426.
Gürgöze, M. and Zeren, S. (2009), "On the Eigencharacteristics of a Centrifugally Stiffened, Visco-Elastic Beam Carrying a Tip Mass", *Proceedings of the Institution of Mechanical Engineers, Part C: Journal of Mechanical Engineering Science*, **223**, 1767-1775.
Gürgöze, M. and Zeren, S. (2011), "The Influences of Both Offset and Mass Moment of Inertia of a Tip Mass on the Dynamics of a Centrifugally Stiffened Visco-Elastic Beam", *Meccanica*, **46**, 1401-1412.
Kumar, A. and Garguli, R. (2009), "Rotating beams and nonrotating beams with shared eigenpair", *Journal of Applied Mechanics*, **76**, 051006:1-051006:14.
Meirovitch, L. (1967), *Analytical Methods in Vibrations*, The MacMillan Company, New York.
Ozdemir Ozgumus, O. and Kaya, M.O. (2010), "Vibration analysis of a rotating tapered Timoshenko beam using DTM", *Meccanica*, **45**, 33-42.
Shahba, A., Attarnejad, R. and Zarrinzadeh, H. (2011), "Free vibration analysis of centrifugally stiffened tapered axially functionally graded beams", *Mechanics of Advanced Materials and Structures*, doi: 10.1080/15376494.2011.627634.
Stevens, K.K. (1966), "On the Parametric Excitation of a Viscoelastic Column", *AIAA Journal*, **4**, 2111-2116.
Wright, A.D., Smith, C.E., Thresher, R.W. and Wang, J.L.C. (1982), "Vibration modes of centrifugally stiffened beams", *Journal of Applied Mechanics*, **49**, 197-202.
Yan, S.X., Zhang, Z.P., Wei, D.J. and Li, X.F. (2011), "Bending vibration of a rotating tapered cantilevers by integral Eq. method", *AIAA Journal*, **49**, 872-876.
Younesian, D. and Esmailzadeh, E. (2010), "Non-linear vibration of variable speed rotating viscoelastic beams", *Nonlinear Dynamics*, **60**, 193-205.
Zarrinzadeh, H., Atternejad, R. and Shahba, A. (2012), "Free vibration of rotating axially functionally graded tapered beams", *Proceedings of the Institution of Mechanical Engineers, Part G: Journal of Aerospace Engineering,* **226**, 363-379.
Zhu, T.L. (2011), "The vibrations of pre-twisted rotating Timoshenko beams by the Rayleigh-Ritz method", *Computational Mechanics*, **47**, 395-408.

Appendix

After substituting expressions (33) and (34) into the differential equation (26), one obtains the following expression

$$\sum_{k=0}^{\infty} C_k (k+r-3)(k+r-2)(k+r-1)(k+r)\bar{x}^{k+r-4} - \eta \sum_{k=0}^{\infty} C_k (k+r-2)(k+r-1)^2 (k+r)\bar{x}^{k+r-3}$$
$$-\frac{a\mu}{3}\sum_{k=0}^{\infty} C_k (k+r-1)(k+r)\bar{x}^{k+r-3} + \frac{1}{2}a(1-\bar{R}\mu)\sum_{k=0}^{\infty} C_k (k+r-1)(k+r)\bar{x}^{k+r}$$
$$+a\bar{R}\sum_{k=0}^{\infty} C_k (k+r-1)(k+r)\bar{x}^{k+r-1} - a\gamma \sum_{k=0}^{\infty} C_k (k+r-1)(k+r)\bar{x}^{k+r-2} - a\mu \sum_{k=0}^{\infty} C_k (k+r)\bar{x}^{k+r+1}$$
$$+a(1-\bar{R}\mu)\sum_{k=0}^{\infty} C_k (k+r)\bar{x}^{k+r} + a\bar{R}\sum_{k=0}^{\infty} C_k (k+r)\bar{x}^{k+r-1} - a\alpha_M (1+\bar{R}+\bar{c})\sum_{k=0}^{\infty} C_k (k+r-1)(k+r)\bar{x}^{k+r-2}$$
$$+b\sum_{k=0}^{\infty} C_k \bar{x}^{k+r} - b\mu \sum_{k=0}^{\infty} C_k \bar{x}^{k+r+1} = 0. \tag{A.1}$$

Collecting the factors of same powers of $\bar{x}$'s leads to

$$\sum_{k=0}^{\infty} C_k (k+r-3)(k+r-2)(k+r-1)(k+r)\bar{x}^{k+r-4} - \eta \sum_{k=0}^{\infty} C_k (k+r-2)(k+r-1)^2 (k+r)\bar{x}^{k+r-3}$$
$$-a\left(\gamma + \alpha_M (1+\bar{R}+\bar{c})\right)\sum_{k=0}^{\infty} C_k (k+r-1)(k+r)\bar{x}^{k+r-2} + a\bar{R}\sum_{k=0}^{\infty} C_k (k+r)^2 \bar{x}^{k+r-1}$$
$$+\frac{1}{2}a(1-\bar{R}\mu)\sum_{k=0}^{\infty} C_k (k+r)(k+r+1)\bar{x}^{k+r} + b\sum_{k=0}^{\infty} C_k \bar{x}^{k+r} - \frac{a\mu}{3}\sum_{k=0}^{\infty} C_k (k+r+2)(k+r)\bar{x}^{k+r+1}$$
$$-b\mu\sum_{k=0}^{\infty} C_k \bar{x}^{k+r+1} = 0. \tag{A.2}$$

After rearranging the above expression, one can write

$$\sum_{k=0}^{\infty} C_k (k+r-3)(k+r-2)(k+r-1)(k+r)\bar{x}^{k+r-4} - \eta \sum_{k=1}^{\infty} C_{k-1} (k+r-3)(k+r-2)^2 (k+r-1)\bar{x}^{k+r-4}$$
$$-a\left(\gamma + \alpha_M (1+\bar{R}+\bar{c})\right)\sum_{k=2}^{\infty} C_{k-2} (k+r-3)(k+r-2)\bar{x}^{k+r-4} + a\bar{R}\sum_{k=3}^{\infty} C_{k-3} (k+r-3)^2 \bar{x}^{k+r-4}$$
$$+\frac{1}{2}a(1-\bar{R}\mu)\sum_{k=4}^{\infty} C_{k-4} (k+r-4)(k+r-3)\bar{x}^{k+r-4} + b\sum_{k=4}^{\infty} C_{k-4} \bar{x}^{k+r-4} - \frac{a\mu}{3}\sum_{k=5}^{\infty} C_{k-5} (k+r-3)(k+r-5)\bar{x}^{k+r-4}$$
$$-b\mu\sum_{k=5}^{\infty} C_{k-5} \bar{x}^{k+r-4} = 0. \tag{A.3}$$

Let us make all summations start at $k = 5$

$$
\begin{aligned}
&C_0(r-3)(r-2)(r-1)(r)\bar{x}^{r-4}+C_1(r-2)(r-1)(r)(r+1)\bar{x}^{r-3}+C_2(r-1)(r)(r+1)(r+2)\bar{x}^{r-2}\\
&+C_3(r)(r+1)(r+2)(r+3)\bar{x}^{r-1}+C_4(r+1)(r+2)(r+3)(r+4)\bar{x}^{r}\\
&+\sum_{k=5}^{\infty}C_k(k+r-3)(k+r-2)(k+r-1)(k+r)\bar{x}^{k+r-4}\\
&-\eta C_0(r-2)(r-1)^2(r)\bar{x}^{r-3}-\eta C_1(r-1)(r)^2(r+1)\bar{x}^{r-2}-\eta C_2(r)(r+1)^2(r+2)\bar{x}^{r-1}\\
&-\eta C_3(r+1)(r+2)^2(r+3)\bar{x}^{r}-\eta\sum_{k=5}^{\infty}C_{k-1}(k+r-3)(k+r-2)^2(k+r-1)\bar{x}^{k+r-4}\\
&-a\left(\gamma+\alpha_M\left(1+\bar{R}+\bar{c}\right)\right)\Big\{C_0(r-1)(r)\bar{x}^{r-2}+C_1(r)(r+1)\bar{x}^{r-1}\\
&+C_2(r+1)(r+2)\bar{x}^{r}+\sum_{k=5}^{\infty}C_{k-2}(k+r-3)(k+r-2)\bar{x}^{k+r-4}\Big\}\\
&+aR\left[C_0(r)^2\bar{x}^{r-1}+C_1(r+1)^2\bar{x}^{r}+\sum_{k=5}^{\infty}C_{k-3}(k+r-3)^2\bar{x}^{k+r-4}\right]\\
&+\frac{1}{2}a(1-\bar{R}\mu)\left[C_0(r)(r+1)\bar{x}^{r}+\sum_{k=5}^{\infty}C_{k-4}(k+r-4)(k+r-3)\bar{x}^{k+r-4}\right]\\
&+b\left[C_0\bar{x}^{r}+\sum_{k=5}^{\infty}C_{k-4}\bar{x}^{k+r-4}\right]-\frac{a\mu}{3}\sum_{k=5}^{\infty}C_{k-5}(k+r-3)(k+r-5)\bar{x}^{k+r-4}\\
&-b\mu\sum_{k=5}^{\infty}C_{k-5}\bar{x}^{k+r-4}=0.
\end{aligned}
\tag{A.4}
$$

Collecting the coefficients of same power of $\bar{x}$ leads to

$$
\begin{aligned}
&C_0(r-3)(r-2)(r-1)(r)\bar{x}^{r-4}+\left\{C_1(r-2)(r-1)(r)(r+1)-\eta C_0(r-2)(r-1)^2(r)\right\}\bar{x}^{r-3}\\
&+\left\{C_2(r-1)(r)(r+1)(r+2)-\eta C_1(r-1)(r)^2(r+1)-a\left(\gamma+\alpha_M\left(1+\bar{R}+\bar{c}\right)\right)C_0(r-1)(r)\right\}\bar{x}^{r-2}\\
&+\left\{C_3(r)(r+1)(r+2)(r+3)-\eta C_2(r)(r+1)^2(r+2)\right.\\
&\left.-a\left(\gamma+\alpha_M\left(1+\bar{R}+\bar{c}\right)\right)C_1(r)(r+1)+aRC_0(r)^2\right\}\bar{x}^{r-1}\\
&+\left\{C_4(r+1)(r+2)(r+3)(r+4)-\eta C_3(r+1)(r+2)^2(r+3)\right.\\
&\left.-a\left(\gamma+\alpha_M\left(1+\bar{R}+\bar{c}\right)\right)C_2(r+1)(r+2)+a\bar{R}C_1(r+1)^2+\frac{1}{2}a(1-\bar{R}\mu)C_0(r)(r+1)+bC_0\right\}\bar{x}^{r}\\
&+\sum_{k=5}^{\infty}\left\{C_k(k+r-3)(k+r-2)(k+r-1)(k+r)-\eta C_{k-1}(k+r-3)(k+r-2)^2(k+r-1)\right.\\
&-a\left(\gamma+\alpha_M\left(1+\bar{R}+\bar{c}\right)\right)C_{k-2}(k+r-3)(k+r-2)+a\bar{R}C_{k-3}(k+r-3)^2\\
&\left.+\frac{1}{2}a(1-\bar{R}\mu)C_{k-4}(k+r-4)(k+r-3)+bC_{k-4}-\frac{a\mu}{3}C_{k-5}(k+r-3)(k+r-5)-b\mu C_{k-5}\right\}\bar{x}^{k+r-4}=0.
\end{aligned}
\tag{A.5}
$$

One can obtain the following relationships, after equating the coefficients of the same power of $\bar{x}$ to zero

$$
\begin{aligned}
&C_0(r-3)(r-2)(r-1)(r)=0,\\
&C_1(r-2)(r-1)(r)(r+1)-\eta C_0(r-2)(r-1)^2(r)=0,\\
&C_2(r-1)(r)(r+1)(r+2)-\eta C_1(r-1)(r)^2(r+1)-a\left(\gamma+\alpha_M\left(1+\bar{R}+\bar{c}\right)\right)C_0(r-1)(r)=0,\\
&C_3(r)(r+1)(r+2)(r+3)-\eta C_2(r)(r+1)^2(r+2)\\
&\quad -a\left(\gamma+\alpha_M\left(1+\bar{R}+\bar{c}\right)\right)C_1(r)(r+1)+aRC_0(r)^2=0,\\
&C_4(r+1)(r+2)(r+3)(r+4)-\eta C_3(r+1)(r+2)^2(r+3)\\
&\quad -a\left(\gamma+\alpha_M\left(1+\bar{R}+\bar{c}\right)\right)C_2(r+1)(r+2)+a\bar{R}C_1(r+1)^2+\frac{1}{2}a\left(1-\bar{R}\mu\right)C_0(r)(r+1)+bC_0=0.
\end{aligned}
\tag{A.6}
$$

The above relationships depending on r represent the recurrence formulae (35) and (37-40) for the unknown coefficients $C_n{}^r$.